# Reconstruction of bi-isotropic material parameters using transient electromagnetic fields

Rikte, Sten

1994

CODEN:LUTEDX/(TEAT-7033)/1-22/(1994)

# Reconstruction of bi-isotropic material parameters using transient electromagnetic fields

**Sten Rikte**

Department of Electroscience
Electromagnetic Theory
Lund Institute of Technology
Sweden

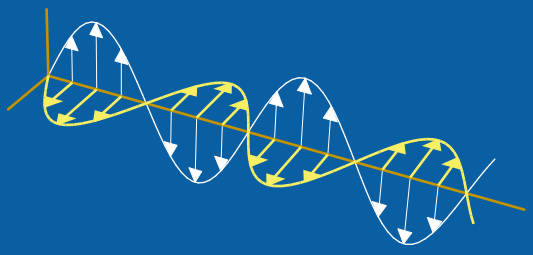

Sten Rikte

Department of Electromagnetic Theory
Lund Institute of Technology
P.O. Box 118
SE-221 00 Lund
Sweden

Editor: Gerhard Kristensson

**Abstract**

In this article, a non-iterative method for solving the transient electromagnetic inverse scattering problem for a homogeneous, dispersive bi-isotropic slab is considered. The slab is excited by a normally incident transverse pulse. The inverse scattering problem is to determine (finite time traces of) the susceptibility kernels, i.e., the four integral kernels present in the constitutive relations, given (finite time traces of) the reflection and transmission kernels, which are obtained by deconvolution of the scattered fields. Two numerical examples illustrate the method with noisy data. Finally, the imbedding equations are proved to be uniquely solvable, and the exact solution to the general propagation problem is found. This solution is given as a uniformly convergent series and supports the employed inverse algorithm.

# 1 Introduction

During the last decade, an increasing interest in the employment of chiral, or more generally, bi-isotropic media in electromagnetic devices has been developed, see, e.g., Refs. [2, 11] for a review. The usefulness of these media is due to the further possibilities of design, that the additional parameters, i.e., the chirality and the non-reciprocity, provide. The characteristic feature of the bi-isotropic medium is the twisting of the plane of polarization of an incident linearly polarized plane wave as it propagates through the medium. This effect is known as optical activity, and it originates from the handedness of the microstructure of the medium. A typical example of a bi-isotropic medium in nature is dextrose. In the microwave regime, a bi-isotropic medium can be manufactured, e.g., by placing many right-wound wire helices randomly in an isotropic host. Clearly, this composite medium is isotropic, in contrast to the likewise artificial pseudochiral or $\Omega$ medium, which has an ordered planar structure of metal wires, bent to the form of the Greek letter $\Omega$, and therefore is (bi-)an-isotropic, see Ref. [13]. In both these media, an interesting additional coupling between electric and magnetic phenomena arises, though different in nature, and this coupling is manifested as time convolutions in the constitutive relations in analogy with the modelling of the usual dispersive effects.

In this article, the stress is on the propagation of transient waves in a single homogeneous, dispersive bi-isotropic slab. In particular, the solution of the inverse problem determining a finite time trace of the electromagnetic properties of the bi-isotropic medium from a finite time trace of reflection and transmission data is considered. One advantage of this time-domain approach is that it requires only a finite time window.

Propagation of transient waves in stratified, reciprocal, bi-isotropic slabs at oblique plane wave incidence has been investigated in Ref. [10]. The generic inverse scattering problem for a homogeneous, possibly non-reciprocal, bi-isotropic slab, subject to excitation by a normally incident plane wave, is discussed in Ref. [9]. In the present paper, the problem in Ref. [9] is generalized to the more realistic case,

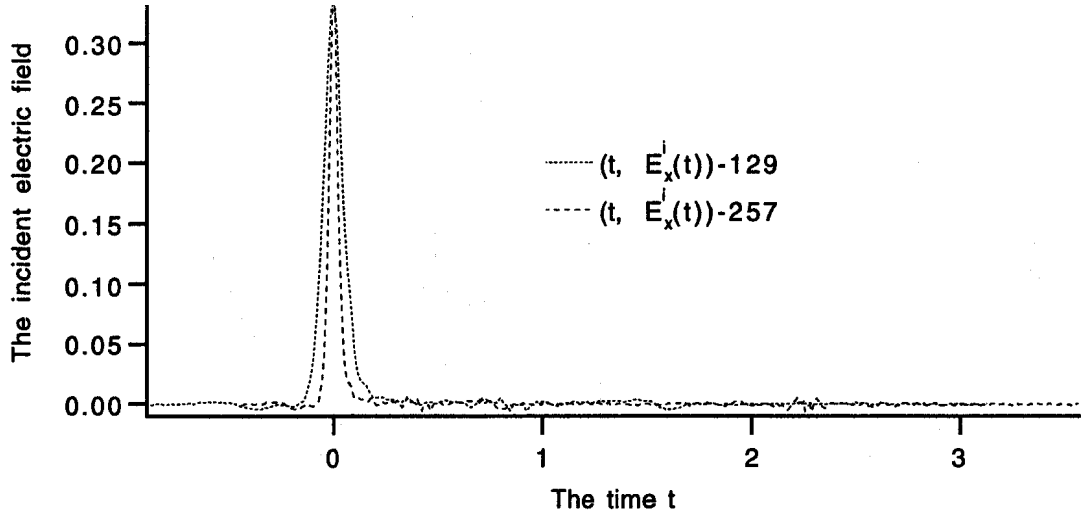


**Figure 1**: The graph of the non-zero component of the incident electric field, $\boldsymbol{E}^i = (E_x^i, E_y^i)$, in the two cases in Example 1 in Section 4. Time $t$ is given in units of $d/c$, while $E_x^i(t)$ is measured in V/m.

where the actual reflected and transmitted electric fields are used as data. The reflection and transmission kernels are independent of the incident plane wave; therefore, when the inverse problem is addressed, the incident electric field can be chosen pertinently. Since a deconvolution always has to be performed, it is preferable to choose the incident pulse as narrow as the experimental technique permits. In fact, pulses with the half-width 50 ps have been generated, see Ref. [6]. In Section 2, the key steps in the derivation of the solution to the wave propagation problem in Ref. [9] are recapitulated. The inverse scattering problem is discussed in Section 3. The improvements in the inverse procedure are illustrated with two numerical examples in Section 4. Finally, in Section 5, the exact solution to the propagation problem is given as infinite series expansions. The specific form increases the understanding of the inverse algorithm used in Section 3. It is also proved that the imbedding and Green functions formulations are equivalent, and that the former — it is already known that the Green functions equations have a unique solution — are uniquely solvable.

# 2 The direct scattering problem

Consider a dispersive bi-isotropic slab occupying the space between the two planes $z = 0$ and $z = d$ in a right-handed Cartesian coordinate system $O(x, y, z)$, where the three basis vectors are denoted by $\boldsymbol{e}_x$, $\boldsymbol{e}_y$, and $\boldsymbol{e}_z$, respectively. For the sake of simplicity, assume that the slab is homogeneous, and that it is surrounded by vacuum with the permittivity $\epsilon_0$, the permeability $\mu_0$, the phase velocity $c = 1/\sqrt{\epsilon_0\mu_0}$, and the wave impedance $\eta = \sqrt{\mu_0/\epsilon_0}$. Furthermore, suppose that there is no mismatch at the boundaries, i.e., the slab has the vacuum permittivity and permeability, and

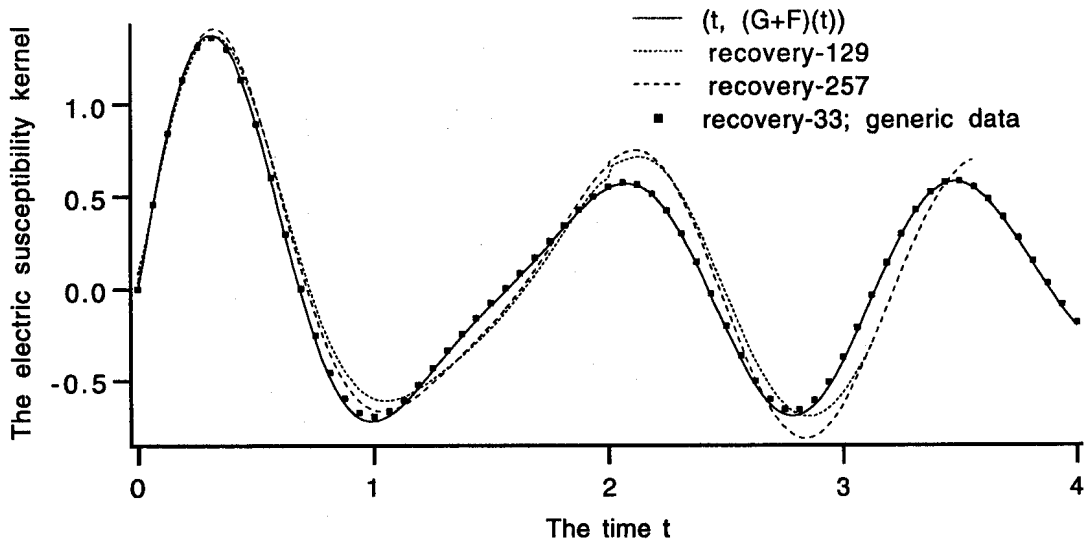


**Figure 2**: The graph of the electric susceptibility kernel, $G+F$, for the homogeneous reciprocal Lorentz medium in Example 1 in Section 4, restricted to two roundtrips. Two reconstructions of this function, performed with 129 and 257 data points per roundtrip, respectively, are also shown in the figure. The recovery based on generic data only, i.e., noise-free scattering kernels is in excellent agreement with the original susceptibility kernel, as indicated by the markers. 33 data points per roundtrip suffice in this latter case. The time scale is given in units of $d/c$, while the vertical axis has the unit $c/d$.

that the constitutive relations at the arbitrary point $\boldsymbol{r} \equiv (x, y, z)$ inside the bi-isotropic slab and at the arbitrary time $t$ are

$$\begin{cases} c\eta \boldsymbol{D}(\boldsymbol{r}, t) = \boldsymbol{E}(\boldsymbol{r}, t) + ((G + F) * \boldsymbol{E})(\boldsymbol{r}, t) + \eta((K + L) * \boldsymbol{H})(\boldsymbol{r}, t), \\ c\boldsymbol{B}(\boldsymbol{r}, t) = ((-K + L) * \boldsymbol{E})(\boldsymbol{r}, t) + \eta \boldsymbol{H}(\boldsymbol{r}, t) + \eta((G - F) * \boldsymbol{H})(\boldsymbol{r}, t), \end{cases}$$

where, e.g., $(G * \boldsymbol{E})(\boldsymbol{r}, t) = \int_{-\infty}^{t} G(t - t')\boldsymbol{E}(\boldsymbol{r}, t')\, dt'$. It is easy to see that these equations hold throughout space provided the susceptibility kernels $G$, $F$, $K$, and $L$ are set equal to zero outside the slab. The kernels $G$ and $F$ model the ordinary dispersive effects of the slab, while the chirality, $K$, and the non-reciprocity, $L$, are the characteristic properties of the bi-isotropic medium. If $L = 0$, the medium is reciprocal, see Ref. [8]. In the interval $t \in [0, \infty)$, the susceptibility kernels $G(t)$, $F(t)$, $K(t)$, and $L(t)$ are assumed to be twice continuously differentiable functions with bounded derivatives. For $t < 0$, they are equal to zero by causality [8].

A right-going transient plane wave, with the electric field $\boldsymbol{E}^i(t)$ at $z = 0$ at time $t$, impinges normally on the slab, which is assumed to be quiescent before a certain time. Suppose that $\boldsymbol{E}^i$ is continuously differentiable with bounded derivative, except possibly at a finite number of (discrete) times, and that this electric field is initially quiescent. The investigation in Ref. [12] guarantees the existence of a transverse solution, independent of the transverse variables $(x, y)$, to the source-free Maxwell

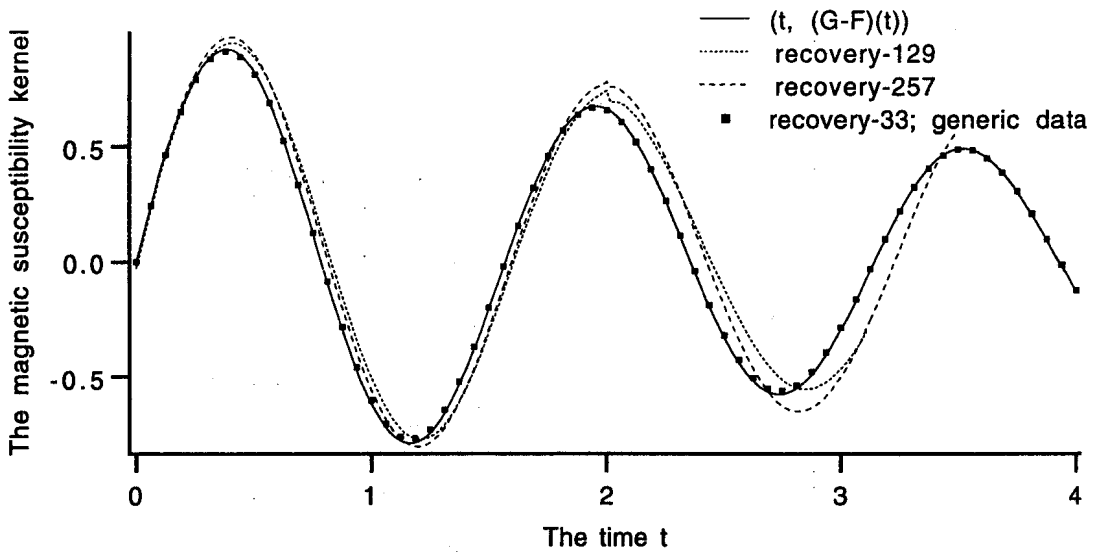


**Figure 3**: The graph of the magnetic susceptibility kernel, $G - F$, for the homogeneous reciprocal Lorentz medium in Example 1 in Section 4, restricted to two roundtrips. See Figure 2 for comments.

equations, $\nabla \times \boldsymbol{E} = -\partial_t \boldsymbol{B}$ and $\nabla \times \boldsymbol{H} = \partial_t \boldsymbol{D}$, in each bounded time interval:

$$\boldsymbol{E}(\boldsymbol{r}, t) = \boldsymbol{e}_x E_x(z,t) + \boldsymbol{e}_y E_y(z,t) \equiv \begin{pmatrix} E_x(z,t) \\ E_y(z,t) \end{pmatrix},$$

and similarly for all the other electromagnetic fields. It is shown that the solution is unique, that the wave front speed is precisely $c$ throughout space, and that the internal and scattered electromagnetic fields inherit the regularity of the incident wave. The reflected and transmitted electric fields at the front and back walls, $z = 0$ and $z = d$, respectively, are denoted by $\boldsymbol{E}^r(t)$ and $\boldsymbol{E}^t(t)$ at the time $t$.

The source-free Maxwell equations for the medium read

$$c\frac{\partial}{\partial z}\begin{pmatrix} \boldsymbol{E} \\ \eta \mathbf{J}\boldsymbol{H} \end{pmatrix} = \frac{\partial}{\partial t}\left\{ \begin{pmatrix} (-\mathbf{K}+\mathbf{L})* & \mathbf{I}+(\mathbf{G}-\mathbf{F})* \\ \mathbf{I}+(\mathbf{G}+\mathbf{F})* & -(\mathbf{K}+\mathbf{L})* \end{pmatrix} \begin{pmatrix} \boldsymbol{E} \\ \eta \mathbf{J}\boldsymbol{H} \end{pmatrix} \right\}, \tag{2.1}$$

where the $2 \times 2$-matrices $\mathbf{I}$ and $\mathbf{J}$ are defined by

$$\mathbf{I} = \begin{pmatrix} 1 & 0 \\ 0 & 1 \end{pmatrix}, \qquad \mathbf{J} = \boldsymbol{e}_z \times \mathbf{I} = \begin{pmatrix} 0 & -1 \\ 1 & 0 \end{pmatrix},$$

and the susceptibility matrices are given by $\mathbf{G} = G\mathbf{I}$, $\mathbf{K} = K\mathbf{J}$, $\mathbf{F} = F\mathbf{I}$, and $\mathbf{L} = L\mathbf{J}$. Define new dependent variables at each point $(z,t)$ through the wave splitting

$$\begin{pmatrix} \boldsymbol{E}^+(z,t) \\ \boldsymbol{E}^-(z,t) \end{pmatrix} = \mathbf{P}\begin{pmatrix} \boldsymbol{E}(z,t) \\ \eta \mathbf{J}\boldsymbol{H}(z,t) \end{pmatrix}, \quad \mathbf{P} = \frac{1}{2}\begin{pmatrix} \mathbf{I} & -\mathbf{I} \\ \mathbf{I} & \mathbf{I} \end{pmatrix}. \tag{2.2}$$

This wave splitting has been employed in several direct and inverse scattering problems for stratified complex slabs, see, e.g., Refs. [3, 4, 9, 10]. For a survey of the well-documented and frequently used wave splitting technique, see Ref. [1].

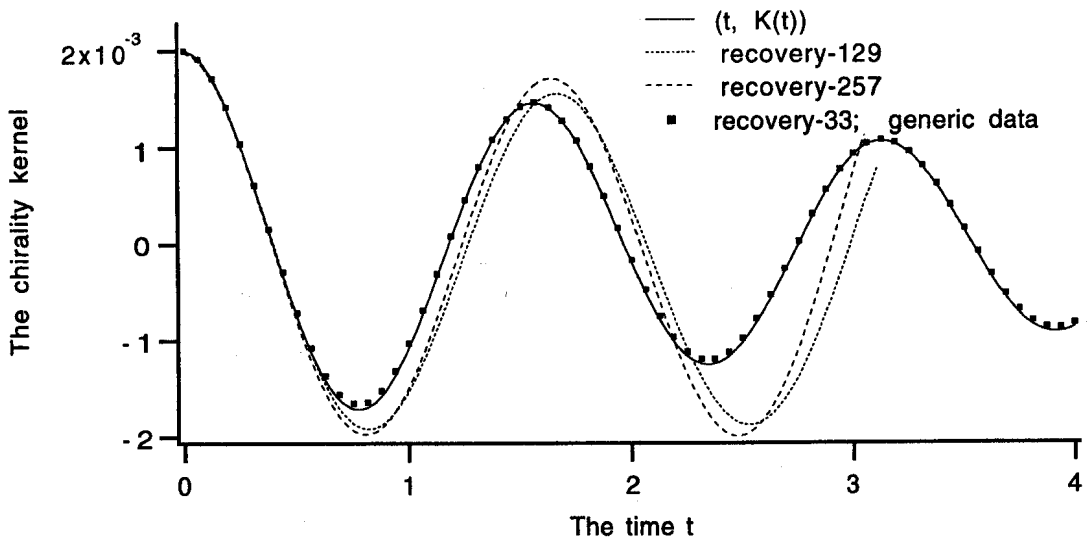


**Figure 4**: The graph of the chirality, $K$, for the homogeneous reciprocal Lorentz medium in Example 1 in Section 4, restricted to two roundtrips. See Figure 2 for comments.

In free space, $\boldsymbol{E}^{\pm}(z,t)$ are the electric fields at $(z,t)$ of the actual right- and left going waves, respectively. As usual in the wave splitting context, such an interpretation is not possible inside the slab. However, since

$$\mathbf{P}^{-1} = \begin{pmatrix} \mathbf{I} & \mathbf{I} \\ -\mathbf{I} & \mathbf{I} \end{pmatrix},$$

the total electric field at the point $(z,t)$ is equal to the sum of the split vector fields at $(z,t)$, and the corresponding total magnetic field is proportional to the difference (with the proportionality matrix $\mathbf{J}/\eta$). Combination of the wave equation (2.1) and the wave splitting (2.2) yields the dynamic equation for the split vector fields $\boldsymbol{E}^{\pm}$:

$$\begin{pmatrix} (c\partial_z + \partial_t)\boldsymbol{E}^+ \\ (c\partial_z - \partial_t)\boldsymbol{E}^- \end{pmatrix} = \frac{\partial}{\partial t}\left\{ \begin{pmatrix} -\mathbf{G}-\mathbf{K} & -\mathbf{F}+\mathbf{L} \\ \mathbf{F}+\mathbf{L} & \mathbf{G}-\mathbf{K} \end{pmatrix} * \begin{pmatrix} \boldsymbol{E}^+ \\ \boldsymbol{E}^- \end{pmatrix} \right\}. \tag{2.3}$$

The free space contribution is recognized as the left term. Since the tangential composants of the electric and magnetic fields are continuous in the $z$-variable throughout space, Eq. (2.2) implies that this holds for the split vector fields also; therefore, the boundary values are $\boldsymbol{E}^+(0,t) = \boldsymbol{E}^i(t)$, $\boldsymbol{E}^-(0,t) = \boldsymbol{E}^r(t)$, $\boldsymbol{E}^+(d,t) = \boldsymbol{E}^t(t)$, and, finally, $\boldsymbol{E}^-(d,t) = \mathbf{0}$, since the slab is excited from the left only.

Elementary analysis of the dynamic equation (2.3) shows that any finite jump-discontinuity $[\boldsymbol{E}^{\pm}(z_1,t)] := \boldsymbol{E}^{\pm}(z_1,t+0) - \boldsymbol{E}^{\pm}(z_1,t-0)$ in $\boldsymbol{E}^{\pm}$ at $(z_1,t)$ is attenuated and rotated as it propagates through the bi-isotropic medium according to

$$[\boldsymbol{E}^{\pm}(z_2, t \pm (z_2-z_1)/c)] = \mathbf{Q}^{\pm}(z_1,z_2)[\boldsymbol{E}^{\pm}(z_1,t)], \tag{2.4}$$

$$\mathbf{Q}^{\pm}(z_1,z_2) = e^{\frac{1}{c}\int_{z_1}^{z_2}(\mp\mathbf{G}(0)-\mathbf{K}(0))dz} = e^{\pm a(z_1,z_2)} \begin{pmatrix} \cos\phi(z_1,z_2) & -\sin\phi(z_1,z_2) \\ \sin\phi(z_1,z_2) & \cos\phi(z_1,z_2) \end{pmatrix},$$

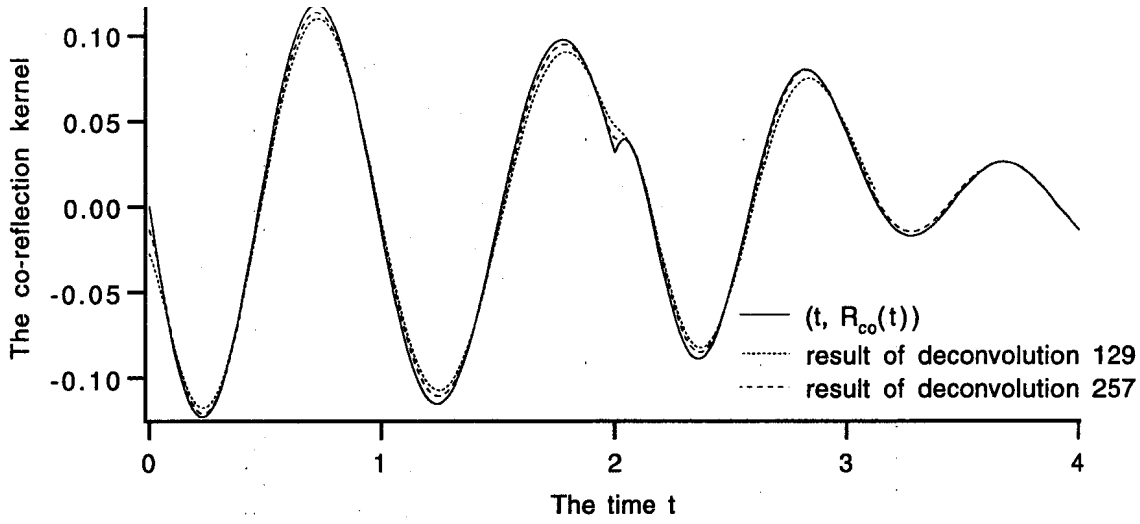


**Figure 5**: The graph of the co-reflection kernel, $R_{\rm co}$, for the homogeneous reciprocal Lorentz medium in Example 1 in Section 4, and its reconstruction in two different cases. These reconstructions have been obtained by the deconvolution of the reflected electric field, $\boldsymbol{E}^r$, see Eq. (2.5), see Figures 8 and 1. Time $t$ is given in units of $d/c$, and the vertical axis in units of $c/d$.

where the rotation angle $\phi(z_1, z_2) = -K(0)(z_2 - z_1)/c$ and the attenuation exponent $a(z_1, z_2) = -G(0)(z_2 - z_1)/c$. The jump-discontinuities in $\boldsymbol{E}^+$ originate from jump-discontinuities in the incident electric field. Jump-discontinuities in $\boldsymbol{E}^-$ never arise in the matched wave impedance case when the excitation from the right is zero.

By Duhamel's principle, the scattering operators can be represented as

$$\begin{cases} \boldsymbol{E}^r(t) = \left(\mathbf{R} * \boldsymbol{E}^i\right)(t), \\ \boldsymbol{E}^t(t + d/c) = \mathbf{Q}^+(0, d)\left\{\boldsymbol{E}^i(t) + \left(\mathbf{T} * \boldsymbol{E}^i\right)(t)\right\}, \end{cases} \tag{2.5}$$

where $\mathbf{R}(t)$ and $\mathbf{T}(t)$ are the reflection and transmission kernels, respectively, at the time $t$. In axially symmetric problems as this one, they have the form

$$\mathbf{R}(t) = \begin{pmatrix} R_{\rm co}(t) & -R_{\rm cross}(t) \\ R_{\rm cross}(t) & R_{\rm co}(t) \end{pmatrix}, \qquad \mathbf{T}(t) = \begin{pmatrix} T_{\rm co}(t) & -T_{\rm cross}(t) \\ T_{\rm cross}(t) & T_{\rm co}(t) \end{pmatrix}.$$

The imbedding equations show that $R_{\rm cross}(t) \equiv 0$ if the medium is reciprocal, see Ref. [10]. If, in addition, $F = 0$, the medium is non-reflective. This follows at once from the dynamic equation (2.3) since the split vector fields are free-coupled in this case.

The Green functions, which essentially are the classical time derivatives of the canonical solutions, i.e., the step responses of the slab from the two different polarizations of the incident electric field, are denoted

$$\mathbf{G}^{\pm}(z, t) = \begin{pmatrix} G_1^{\pm}(z, t) & -G_2^{\pm}(z, t) \\ G_2^{\pm}(z, t) & G_1^{\pm}(z, t) \end{pmatrix}, \tag{2.6}$$

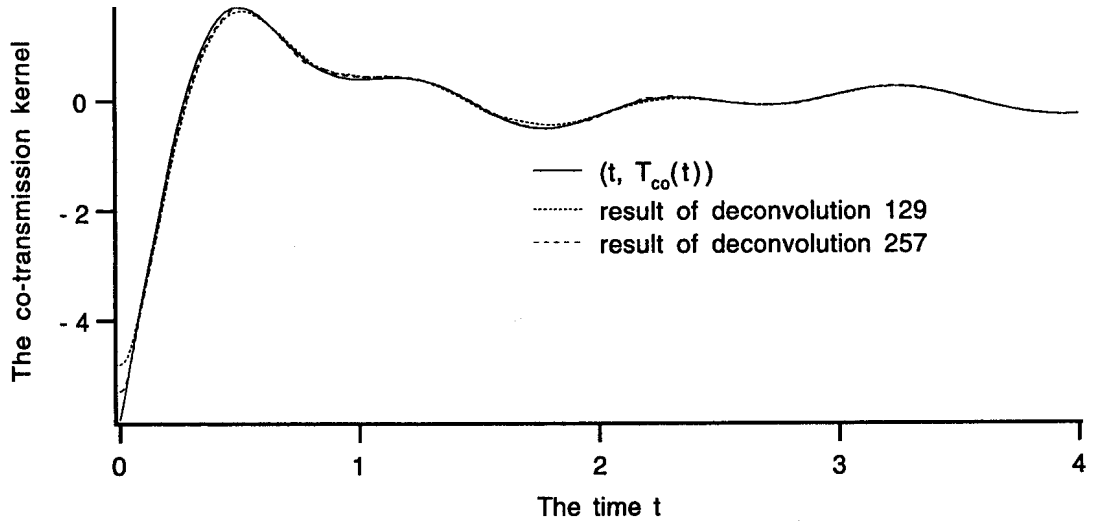


**Figure 6**: The graph of the co-transmission kernel, $T_{\mathrm{co}}$, for the homogeneous reciprocal Lorentz medium in Example 1 in Section 4, and its reconstruction in two different cases. These reconstructions have been calculated by the deconvolution of the transmitted electric field, $\boldsymbol{E}^t$, see Eq. (2.5), see Figures 9, 10, and 1. Time $t$ is given in units of $d/c$.

and they relate the split vector fields $\boldsymbol{E}^{\pm}$ at an arbitrary point $z$ inside the slab to the excitation $\boldsymbol{E}^i$ at the front wall according to

$$\begin{cases} \boldsymbol{E}^+(z,t+z/c) = \mathbf{Q}^+(0,z)\left\{\boldsymbol{E}^+(0,t) + \left(\mathbf{G}^+(z,\cdot) * \boldsymbol{E}^+(0,\cdot)\right)(t)\right\}, \\ \boldsymbol{E}^-(z,t+z/c) = \mathbf{Q}^+(0,z)\left(\mathbf{G}^-(z,\cdot) * \boldsymbol{E}^+(0,\cdot)\right)(t). \end{cases} \tag{2.7}$$

In this definition, Duhamel's principle and the axial symmetry are referred to again. The lack of symmetry in these equations originates from the fact that the wave impedance is matched at the back wall. Furthermore, due to strict causality and the invariance under time translations, $\mathbf{G}^{\pm}(z,t) = \mathbf{0}$ when $t < 0$. The boundary values $\mathbf{G}^+(0,t) = \mathbf{0}$ and $\mathbf{G}^-(d,t) = \mathbf{0}$ follow from the definition of the Green functions and the lack of sources on the right hand side of the slab. Notice that Eq. (2.5) is a special case of Eq. (2.7); therefore, $\mathbf{R}(t) = \mathbf{G}^-(0,t)$ and $\mathbf{T}(t) = \mathbf{G}^+(d,t)$ at each time $t$. The Green functions equations are obtained, e.g., by inserting Eq. (2.7) into Eq. (2.3):

$$c\partial_z\mathbf{G}^+ = -(\partial_t\{\mathbf{G}+\mathbf{K}\}) * \mathbf{G}^+ - \partial_t\left\{\mathbf{G}+\mathbf{K}+(\mathbf{F}-\mathbf{L}) * \mathbf{G}^-\right\},$$
$$c\partial_z\mathbf{G}^- - 2\partial_t\mathbf{G}^- = 2\mathbf{G}(+0)\mathbf{G}^- + \partial_t\left\{\mathbf{F}+\mathbf{L}+(\mathbf{F}+\mathbf{L}) * \mathbf{G}^+\right\} + (\partial_t\{\mathbf{G}-\mathbf{K}\}) * \mathbf{G}^-.$$

For an alternative derivation, see Ref. [12]. These equations hold for $0 < z < d$ and $t > 0$ except on the line $t = 2(d-z)/c$, where $\mathbf{G}^-$ has a finite jump discontinuity:

$$\mathbf{G}^-(z, 2(d-z)/c+0) - \mathbf{G}^-(z, 2(d-z)/c-0) = e^{2a(z,d)}\big(\mathbf{F}(+0)+\mathbf{L}(+0)\big)/2.$$

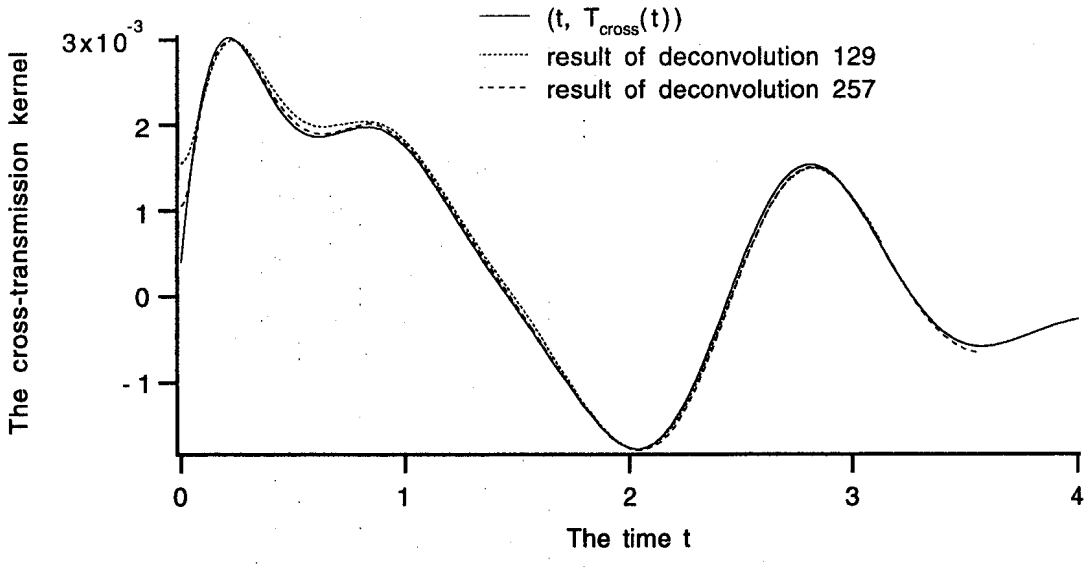


**Figure 7**: The graph of the cross-transmission kernel, $T_{\text{cross}}$, for the homogeneous reciprocal Lorentz medium in Example 1 in Section 4, and its reconstruction in the two discussed cases. See Figure 6 for comments.

The initial values are given by [9]

$$\mathbf{G}^-(z,+0) = -\big(\mathbf{F}(+0) + \mathbf{L}(+0)\big)/2, \tag{2.8}$$

$$2c\mathbf{G}^+(z,+0) = z\left(\mathbf{F}^2(+0) - \mathbf{L}^2(+0) - 2(\mathbf{G}'(+0) + \mathbf{K}'(+0))\right). \tag{2.9}$$

Integration of the Green functions equations along the characteristics and discretization by the trapezoidal rule give efficient numerical algorithms for both the direct and inverse problems. The time step in the discretization is denoted by $\Delta t$ and the step in the spatial variable by $\Delta z = c\Delta t/2$.

In the direct scattering problem, the susceptibility kernels are known, and the scattering kernels, i.e., the reflection and transmission kernels, are computed by solving the Green functions equations or the imbedding equations numerically. The scattered fields, i.e., the reflected and transmitted electric fields, are then easily calculated by Eq. (2.5). In the next section, the inverse problem is treated.

# 3 The inverse scattering problem

The inverse scattering problem for the bi-isotropic slab is to infer information about the susceptibility kernels from finite time traces of the reflected and transmitted electric fields. The first step in the inverse procedure is the deconvolution of the scattered electric fields, $\boldsymbol{E}^r$ and $\boldsymbol{E}^t$. If the duration of the incident pulse is comparatively short and the peak of the pulse occurs at $t = 0$, as in the numerical examples in Section 4, Eq. (2.5) implies that the following simple deconvolution technique

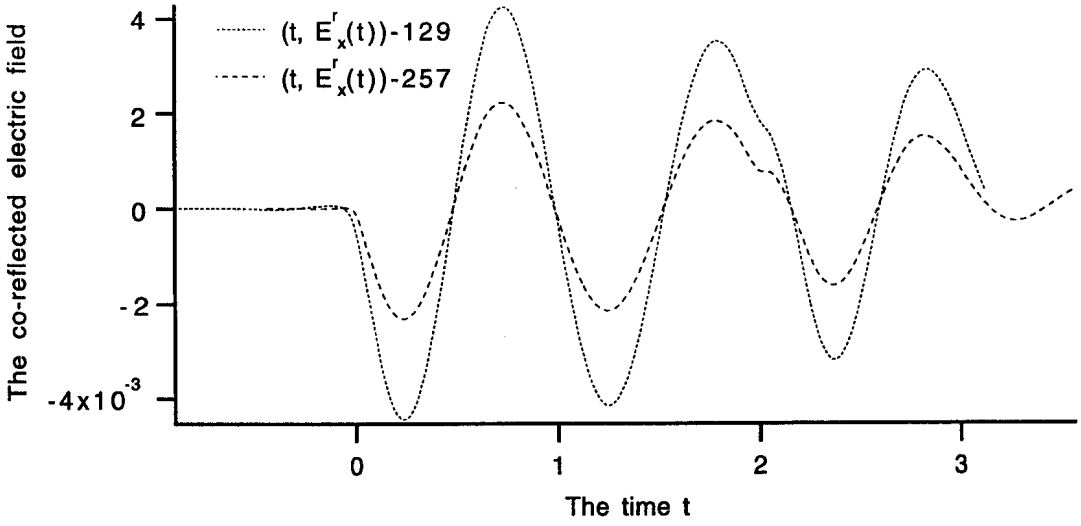


**Figure 8**: The graph of the co-component of the reflected electric field, $\boldsymbol{E}^r = (E^r_x, E^r_y)$, in the two discussed cases in Example 1 in Section 4. Time scale is given in units of $d/c$, and the scattered electric fields have the same unit as the incident electric field in Figure 1.

can be applied:

$$\begin{cases} \boldsymbol{E}^r(t) = \mathbf{R}(t) \displaystyle\int_{-\infty}^{t} \boldsymbol{E}^i(t')\, dt', \quad t \geq 0, \\ \boldsymbol{E}^t(t + d/c) = \mathbf{Q}^+(0,d) \left\{ \boldsymbol{E}^i(t) + \mathbf{T}(t) \displaystyle\int_{-\infty}^{t} \boldsymbol{E}^i(t')\, dt' \right\}, \quad t \geq 0, \\ \boldsymbol{E}^t(-\Delta t + d/c) = \mathbf{Q}^+(0,d) \left\{ \boldsymbol{E}^i(-\Delta t) + \mathbf{T}(0) \displaystyle\int_{-\infty}^{-\Delta t} \boldsymbol{E}^i(t')\, dt' \right\}. \end{cases} \tag{3.1}$$

Initially, the values of $\mathbf{T}(0)$ and $\mathbf{Q}(0,d)$ are obtained by the combination of the third equation and the second, evaluated at $t = 0$. The values of $\mathbf{R}(j) := \mathbf{R}(j\Delta t)$ and $\mathbf{T}(j) := \mathbf{T}(j\Delta t)$ for $j = 0, 1, 2, \ldots, J_{\max}$ then easily follow.

An inverse algorithm is now used to calculate finite time traces of the susceptibility kernels. The initial values $G(0)$ and $K(0)$ follow immediately from Eq. (2.4) and the assumption that the angle $\phi(0,d) = -K(0)d/c$ is less than $2\pi$. The values of $F(0)$ and $L(0)$ are given by Eq. (2.8) since $\boldsymbol{G}^-(+0,+0) = \mathbf{R}(+0)$. The Green functions equations suggest that the inverse algorithm should be based on the derivatives of the susceptibility kernels, rather than these kernels themselves. Karlsson [5, 7] has shown that the forward algorithm can be employed in solving the inverse problem in the special case of an isotropic slab, and this method was extended to the bi-isotropic case in Ref. [9]. A more detailed analysis of the Green functions equations for the related an-isotropic slab shows that this method can be improved, see Fridén [3]. The outline of this improved method is as follows:

**Time step** 0. The second Green functions equation, evaluated at $(+0,+0)$, and the two initial conditions (2.8) and (2.9) yield the following initial values for the

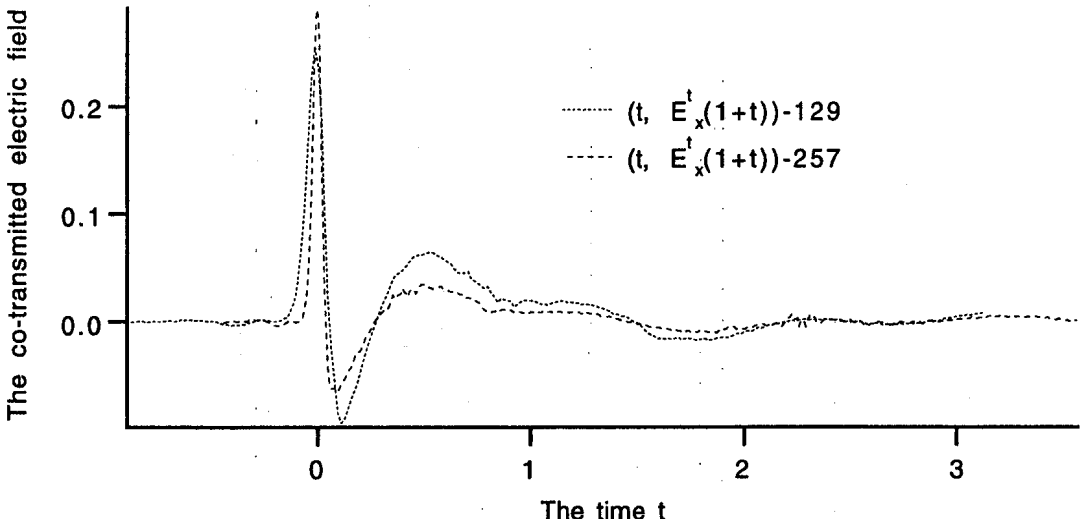


**Figure 9**: The graph of the co-component of the transmitted electric field, $\boldsymbol{E}^t = (E_x^t, E_y^t)$, for the homogeneous reciprocal Lorentz medium in the two cases in Example 1 in Section 4. Time scale is given in units of $d/c$, and the scattered electric fields have the same unit as the incident electric field. Note the time-translation of half a roundtrip in the transmitted electric field components.

derivatives of the susceptibility kernels:

$$\mathbf{G}'(0) + \mathbf{K}'(0) = \frac{1}{2}(\mathbf{F}(0)^2 - \mathbf{L}(0)^2) - \frac{c}{d}\mathbf{T}(0)$$
$$\mathbf{F}'(0) + \mathbf{L}'(0) = -2(\mathbf{R}'(0) + \mathbf{G}(0)\mathbf{R}(0)).$$

**Time step** $J$. Assume that $G'(j)$, $K'(j)$, $F'(j)$, and $L'(j)$ are known at times $j < J$, where $G'(j) := \frac{d}{dt}G(j\Delta t)$, et c. In particular, this means that the values of $\mathbf{G}^{\pm}(i,j) := \mathbf{G}^{\pm}(i\Delta z, j\Delta t)$ at times $j < J$ are known, since the forward program can be applied. The discretized Green functions equations imply that

$$\begin{cases} \mathbf{T}(J) = \mathbf{A}^+\mathbf{G}'(J) + \mathbf{B}^+\mathbf{K}'(J) + \mathbf{C}^+\mathbf{F}'(J) + \mathbf{D}^+\mathbf{L}'(J) + \mathbf{M}^+(J), \\ \mathbf{R}(J) = \mathbf{A}^-\mathbf{G}'(J) + \mathbf{B}^-\mathbf{K}'(J) + \mathbf{C}^-\mathbf{F}'(J) + \mathbf{D}^-\mathbf{L}'(J) + \mathbf{M}^-(J), \end{cases} \tag{3.2}$$

where the coefficients $\mathbf{A}^{\pm}$, $\mathbf{B}^{\pm}$, $\mathbf{C}^{\pm}$, and $\mathbf{D}^{\pm}$ are constant matrices. The matrices $\mathbf{M}^{\pm}$ depend on $G'(j)$, $K'(j)$, $F'(j)$, and $L'(j)$ at times $j < J$ only. All these matrices have the form (2.6). By running the forward program at time $J$ with $G'(J) = K'(J) = F'(J) = L'(J) = 0$, one obtains the values of $\mathbf{M}^{\pm}(J)$ as the dummy values of $\mathbf{T}(J)$ and $\mathbf{R}(J)$, respectively. The linear system (3.2) in $G'(J)$, $K'(J)$, $F'(J)$, and $L'(J)$ can be solved since the real values of $\mathbf{T}(J)$ and $\mathbf{R}(J)$ are known by the deconvolution (3.1) above. Finally, $\mathbf{G}^{\pm}(i,J)$ are computed at all the grid points $(i,J)$ by running the forward program at time $J$ once again, this time with respect to the correct values of $G'(J)$, $K'(J)$, $F'(J)$, and $L'(J)$.

The procedure for the time step $J$ is repeated for the steps $J+1, \ldots, J_{\max}$. Finally, the susceptibility kernels are obtained from its time derivatives by numerical integration.

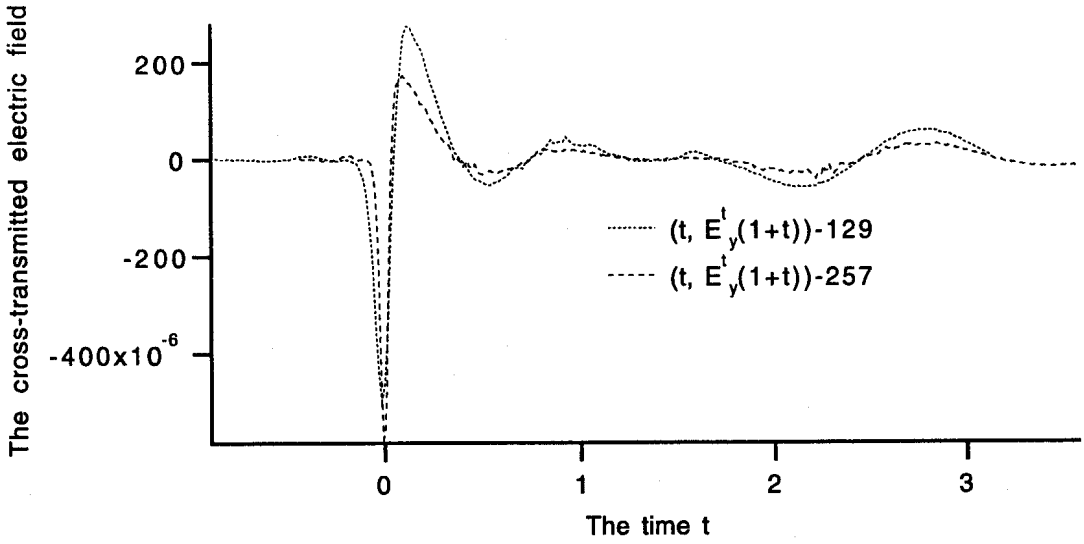


**Figure 10**: The graph of the cross-component of the transmitted electric field, $\boldsymbol{E}^t = (E_x^t, E_y^t)$, for the homogeneous reciprocal Lorentz medium in the two cases in Example 1 in Section 4. See Figure 9 for comments.

The continuous counterpart to Eq. (3.2) is

$$\begin{cases} \mathbf{T}(t) = -\Big(\mathbf{G}'(t) + \mathbf{K}'(t) - \dfrac{(\mathbf{F}(0) - \mathbf{L}(0))(\mathbf{F}(t) + \mathbf{L}(t))}{2}\Big)\dfrac{d}{c} + \text{integral terms}, \\ \mathbf{R}(t) = -\dfrac{\mathbf{F}(t) + \mathbf{L}(t)}{2} + \text{integral terms}. \end{cases} \tag{3.3}$$

In Section 5, these equations are derived with the aid of the imbedding equations. Roughly speaking, all new information about the co-susceptibility kernel $F$ and the non-reciprocity kernel $L$ is obtained from the co- and cross reflection kernels, respectively. Using this information, the changes in the co-susceptibility kernel $G$ and the chirality kernel $K$ can be deduced from the co- and cross transmission kernels, respectively.

By discretizing the integrals in Eq. (3.3) and by employing approximations such as $F'(t) = (F(t) - F(t - \Delta t)/\Delta t$, the coefficient matrices $\mathbf{A}^{\pm}$, $\mathbf{B}^{\pm}$, $\mathbf{C}^{\pm}$, and $\mathbf{D}^{\pm}$ in Eq. (3.2) can be obtained explicitly. Note that $\mathbf{A}^-$, $\mathbf{B}^-$, $\mathbf{C}^{\pm}$, and $\mathbf{D}^{\pm}$ all tend to zero as $\Delta t$ tends to zero, and that $\mathbf{A}^-$ and $\mathbf{B}^-$ tend to zero one order faster than $\mathbf{C}^-$ and $\mathbf{D}^-$. In the limit, new information about $F$ and $L$ obviously is contained the matrices $\mathbf{M}^{\pm}$.

# 4 Numerical examples

In the following two examples, the numerical performance of the algorithm is demonstrated.

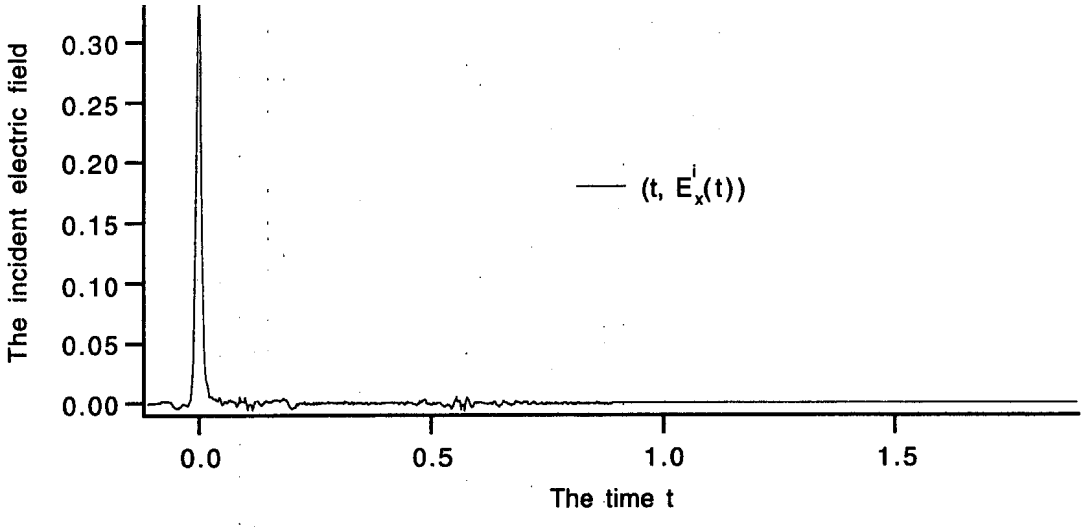


**Figure 11**: The graph of the non-zero component of the incident electric field, $\boldsymbol{E}^i = (E_x^i, E_y^i)$, employed in Example 2 in Section 4. Time $t$ is given in units of $d/c$, while $E_x^i(t)$ is measured in V/m.

**Example** 1. A reciprocal homogeneous Lorentz medium with the susceptibilities

$$\begin{cases} G(t) = e^{-0.2t}\sin 4t + 0.3e^{-0.5t}\sin 6t, \\ F(t) = 0.3e^{-0.5t}\sin 6t, \\ K(t) = 0.002e^{-0.2t}\cos 4t, \end{cases}$$

(and $L(t) \equiv 0$) is investigated in this first example. All numerical values of the kernels are given in the unit $c/d$ and time $t$ in units of $d/c$. The restrictions of these susceptibility kernels to two roundtrips, i.e, the interval $[0, 4]$ are depicted in Figures 2, 3, and 4. Note that the chirality, $K$, is approximately three orders of magnitude smaller than the electric susceptibility $G + F$.

Two incident pulses are depicted in Figure 1. They are examples of realistic experimental pulses. 129 and 257 data points per roundtrip are employed in these two cases, respectively. Data relevant for the inverse scattering problem is shown in Figures 8, 9, and 10. The result of the deconvolution of the scattered electric fields is shown in Figures 5, 6, and 7. By use of the imbedding equations, one can show that $R_{\text{cross}} = 0$ in reciprocal cases. These quantities are used in the inverse procedure, and the reconstructions of the susceptibility kernels are shown in Figures 2, 3, and 4 for the two incident pulses. Notice that the agreement is excellent already at 33 data points per roundtrip, provided the noise-free reflection and transmission kernels are employed in the inverse procedure instead of the scattered electric fields in Figures 8, 9, and 10. (In this case, the exact values of $G(0)$ and $K(0)$ are assumed to be known.) This indicates that effort should be made in the generation of sharp pulses, rather than in increasing the number of data points.

**Example** 2. A non-reciprocal Debye-Lorentz medium is considered. With all frequencies given in units of $c/d$ and time $t$ given in units of $d/c$, the susceptibility

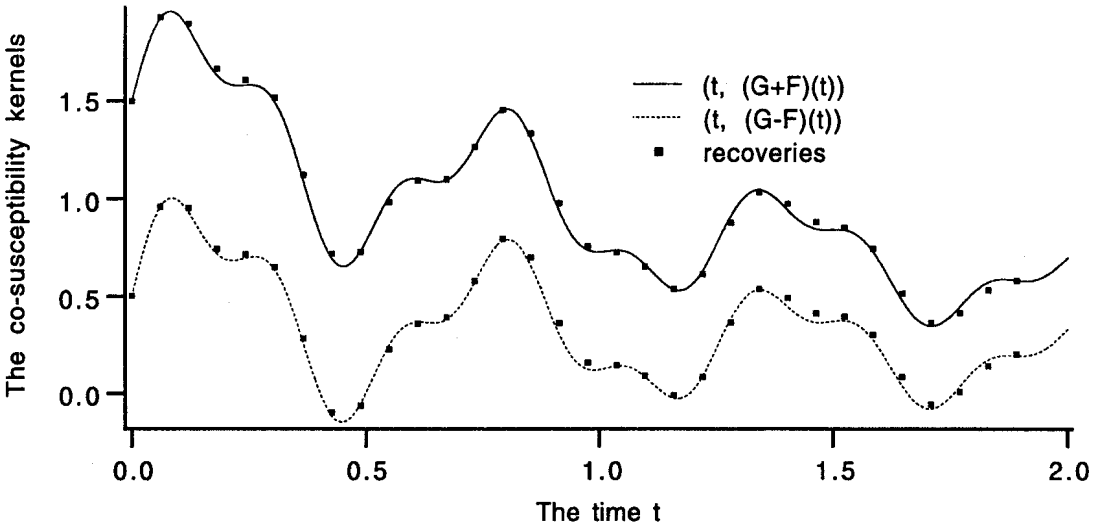


**Figure 12**: The graphs of the electric and magnetic susceptibilities, $G + F$ and $G - F$, respectively, for the Debye-Lorentz medium in Example 2 in Section 4, restricted to one roundtrip. Time $t$ is given in units of $d/c$, while the vertical axis is given in units of $c/d$.

kernels are

$$\begin{cases} G(t) = e^{-0.5t} + 0.5e^{-0.5t}\sin 10t + 0.2e^{-0.5t}\sin 25t, \\ F(t) = 0.5e^{-0.5t}, \\ K(t) = 0.02e^{-0.5t}\cos 10t + 0.1e^{-0.5t}\cos 25t, \\ L(t) = 0.01e^{-0.5t}\cos 10t. \end{cases}$$

This medium has more and higher resonance frequencies than the pure Lorentz medium in Example 1. In order to obtain good results in this case, only one roundtrip is considered, i.e, the interval $[0, 2]$. The restriction to one roundtrip is not a serious limitation, since one can extract more information by choosing a thicker slab consisting of the same medium. In total, 1025 data points are used in this second example. The susceptibility kernels are depicted in Figures 12 and 13, while the incident pulse is found in Figure 11. Reflection and transmission data for this medium are shown in Figures 16 and 17, respectively. These electric fields have been computed by solving the Green functions equations or the imbedding equations followed by convolution, see Eq. (2.5). The result of the introductory deconvolution is depicted in Figures 14 and 15. In spite of the incompleteness of deconvolution, the reconstructions of the susceptibility kernels is excellent, which indicates that the method is stable under perturbations. The recovered susceptibility kernels are also found in Figures 12 and 13, represented by markers. These reconstructions are practically indistinguishable from the real ones.

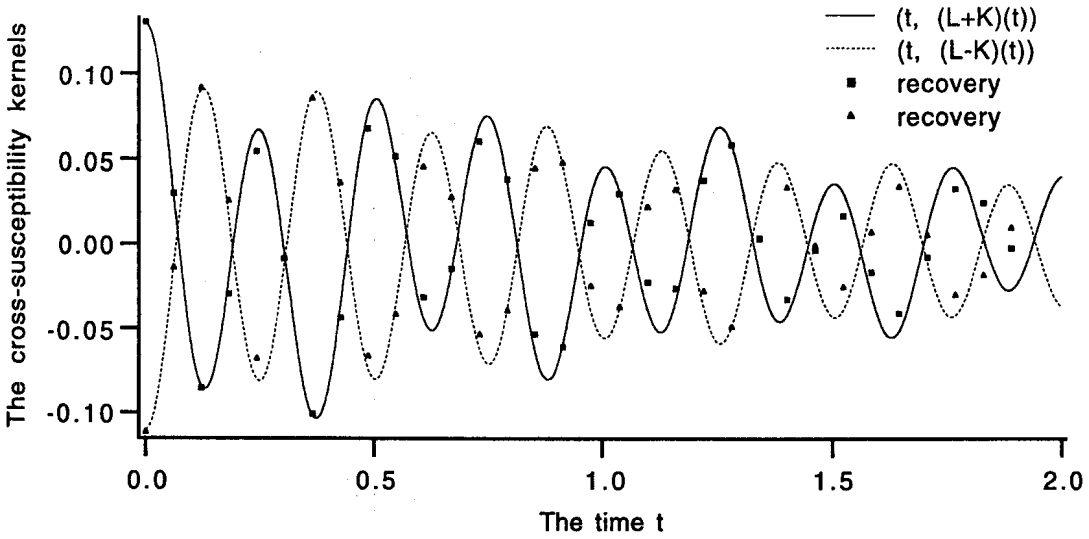


**Figure 13**: The graphs of the magneto-electric susceptibility kernels, $L \pm K$, for the Debye-Lorentz medium in Example 2 in Section 4, restricted to one roundtrip. See Figure 12 for comments.

# 5 Exact solutions

In this section, the exact solution to the propagation problem treated above is derived. It is shown that for each given time $a > 0$, both $\mathbf{G}^+(z,t)$ and $\mathbf{G}^-(z,t)$ can be written as infinate series that converge absolutely and uniformly on the set $\{(z,t) \in (0,d) \times (0,a) : t \neq 2(d-z)/c\}$. The result holds for each set $(G(t), K(t), F(t), L(t)), t \in [0,\infty)$ of bounded and twice continuously differentiable susceptibility kernels with bounded derivatives. As mentioned before, the explicit form of the solution strongly supports Karlsson's extended method for the inverse scattering problem. The derivation is based on the imbedding method, which is an alternative formulation of the propagation problem, that also relies on the dynamic equation (2.3) and Duhamel's principle. As an intermediate step, it is shown, that each solution to the Green functions equations, via a well-defined transformation between the two formulations of the propagation problem, can be regarded as a solution to the imbedding equations, and vice versa. This establishes the fact that the latter equations also are uniquely solvable (in each bounded time interval). Furthermore, the solution to the imbedding equations is given explicitly.

Introduce travel time coordinates $(x,s)$ by $x = z/d$ and $s = tc/d$, and define dimensionless Green functions and susceptibility kernels by the following abuse of notation: $\mathbf{G}^{\pm}(x,s) := \mathbf{G}^{\pm}(z,t)d/c$, $G(s) := G(t)d/c$ et c. The equation for $\mathbf{G}^-(x,s)$ can then be written as

$$\begin{aligned}(\partial_x - 2\partial_s)\mathbf{G}^- = (\mathbf{G}(0) + \mathbf{K}(0))\mathbf{G}^- + \\ + \partial_s\left\{(\mathbf{I} + \mathbf{G}^+ *)(\mathbf{F} + \mathbf{L}) + \mathbf{G}^- * (\mathbf{G} - \mathbf{K})\right\},\end{aligned} \tag{5.1}$$

and the equation for $\mathbf{G}^+(x,s)$ becomes

$$-\partial_x \mathbf{G}^+ = (\mathbf{I} + \mathbf{G}^+ *)(\mathbf{G}' + \mathbf{K}') + \partial_s\left\{(\mathbf{F} - \mathbf{L}) * \mathbf{G}^-\right\}. \tag{5.2}$$

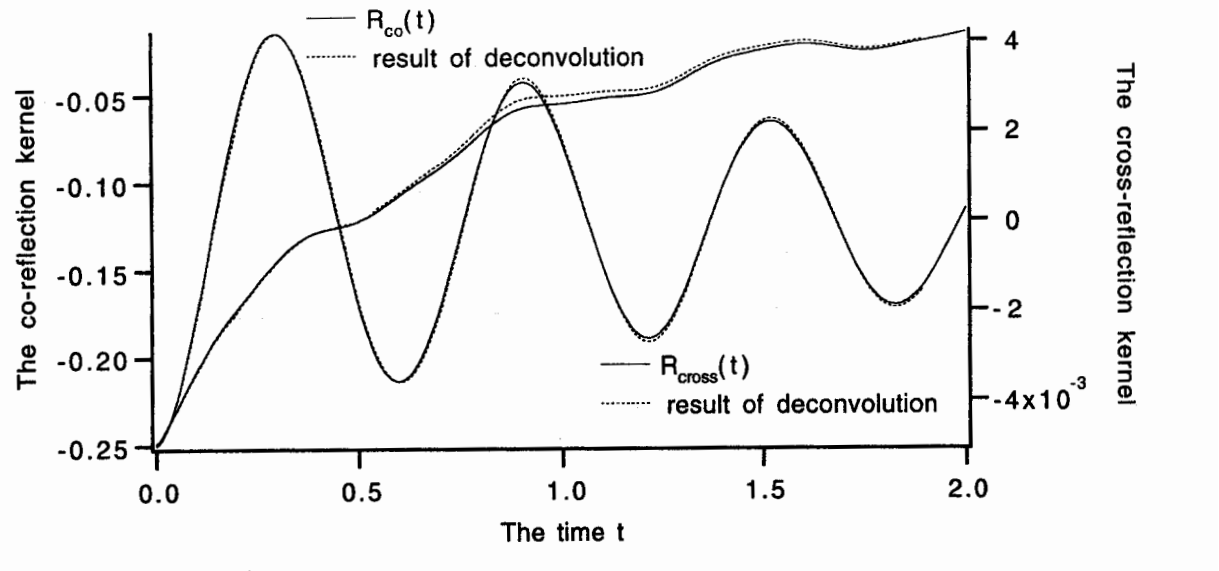


**Figure 14**: The graphs of the reflection kernels, $R_{\rm co}$ and $R_{\rm cross}$, for the Debye-Lorentz medium in Example 2 in Section 4. The broken lines give the reconstructions obtained by deconvolution of the reflected electric field, see Eq. (2.5). See also Figures 11 and 16. Time $t$ is given in units of $d/c$, and the vertical axis in units of $c/d$.

The investigation in Ref. [12] shows that the Green functions equations are uniquely solvable; therefore, it is possible to define new dependent variables, $\mathbf{R}(x,s)$ and $\mathbf{T}(x,s)$, on the same form and with the same regularity as $\mathbf{G}^-(x,s)$ and $\mathbf{G}^+(x,s)$, respectively, by the Volterra equations

$$\begin{cases} \mathbf{G}^+(1,s) = \mathbf{G}^+(x,s) + \mathbf{T}(x,s) + \big(\mathbf{T}(x,\cdot) * \mathbf{G}^+(x,\cdot)\big)(s) = \mathbf{T}(0,s), \\ \mathbf{G}^-(x,s) = \mathbf{R}(x,s) + \big(\mathbf{R}(x,\cdot) * \mathbf{G}^+(x,\cdot)\big)(s). \end{cases} \tag{5.3}$$

The functions $\mathbf{R}(x,s)$ and $\mathbf{T}(x,s)$ are uniquely determined by Eq. (5.3) and they are known as the reflection and transmission imbedding kernels, respectively, for the subsection $[x,1]$ of the physical slab $[0,1]$, see Ref. [9]. Conversely, the Green functions $\mathbf{G}^\pm(x,s)$ are determined uniquely by Eq. (5.3) when the imbedding kernels are given. Note that the functions $\mathbf{R}(x,s)$ and $\mathbf{T}(x,s)$ defined by Eq. (5.3) become continuously differentible except on the line $s = 2(1-x)$, where $\mathbf{R}(x,s)$ has a finite jump-discontinuity, and, furthermore, that $\mathbf{R}(s) := \mathbf{R}(0,s)$ and $\mathbf{T}(s) := \mathbf{T}(0,s)$ are the physical reflection and transmission kernels, respectively, at time $s$.

Formally, the imbedding kernels are defined by:

$$\begin{cases} \boldsymbol{E}^-(z,t) = \big(\mathbf{R}(z,\cdot) * \boldsymbol{E}^+(z,\cdot)\big)(t) \\ \boldsymbol{E}^+(d,t+(d-z)/c) = \mathbf{Q}^+(z,d)\left\{\boldsymbol{E}^+(z,t) + \big(\mathbf{T}(z,\cdot) * \boldsymbol{E}^+(z,\cdot)\big)(t)\right\}, \end{cases}$$

where $\mathbf{R}(x,s) = \mathbf{R}(z,t)d/c$ and $\mathbf{T}(x,s) = \mathbf{T}(z,t)d/c$. A straightforward derivation using the dynamic equation (2.3) shows that the imbedding kernels satisfy the non-

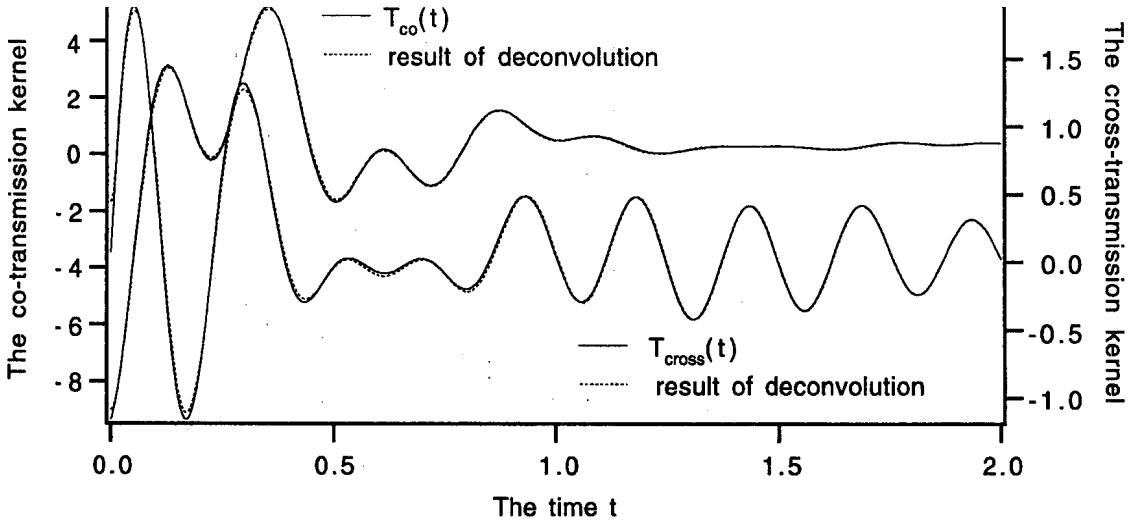


**Figure 15**: The graphs of the transmission kernels, $T_{\rm co}$ and $T_{\rm cross}$, for the Debye-Lorentz medium in Example 2 in Section 4. The reconstructions have been obtained by deconvolution of the transmitted electric field, see Eq. (2.5). See also Figures 11 and 17. Time $t$ is given in units of $d/c$, and the vertical axis in units of $c/d$.

linear partial integro-differential equations

$$\begin{aligned}
&\partial_x \mathbf{R} - 2\partial_s \mathbf{R} = \partial_s \left\{ \mathbf{F} + \mathbf{L} + 2\mathbf{G} * \mathbf{R} + (\mathbf{F} - \mathbf{L}) * \mathbf{R} * \mathbf{R} \right\} \\
&\mathbf{R}(1, s) = \mathbf{0} \\
&\mathbf{R}(x, +0) = -\big(\mathbf{F}(+0) + \mathbf{L}(+0)\big)/2 \\
&[\mathbf{R}(x, 2(1-x))] = \frac{\exp\big(2a(x,1)\big)}{2} \big(\mathbf{F}(+0) + \mathbf{L}(+0)\big)
\end{aligned} \tag{5.4}$$

and

$$\begin{aligned}
&\partial_x \mathbf{T} = (\partial_s \{\mathbf{G} + \mathbf{K}\}) * \mathbf{T} + \partial_s \{\mathbf{G} + \mathbf{K} + (\mathbf{F} - \mathbf{L}) * (\mathbf{R} + \mathbf{R} * \mathbf{T})\} \\
&\mathbf{T}(1, s) = \mathbf{0} \\
&2\mathbf{T}(x, +0) = \left\{ \mathbf{F}^2(+0) - \mathbf{L}^2(+0) - 2(\mathbf{G}'(+0) + \mathbf{K}'(+0)) \right\} (1 - x)
\end{aligned} \tag{5.5}$$

where the attenuation factor $a(x_1, x_2) = -(x_2 - x_1)G(+0)$. The domain of definition for these equations is $\{(x, s) : s > 0,\, 0 < x < 1,\, s \neq 2(1-x)\}$. Note that the reflection imbedding kernel is independent of the chirality kernel $\mathbf{K}$.

In this paragraph, the imbedding equations are derived from the Green functions equations (5.1)–(5.2) and the relation (5.3) between the two formulations, which is considered to be the definition of the imbedding kernels. Differentiation with respect to $x$ in the first relation of Eq. (5.3) yields

$$(\mathbf{I} + \mathbf{G}^+ *)\partial_x \mathbf{T} = -(\mathbf{I} + \mathbf{T} *)\partial_x \mathbf{G}^+. \tag{5.6}$$

Analogously, differentiation of the second relation in Eq. (5.3) gives the equation

$$(\partial_x - 2\partial_s)\mathbf{G}^- = (\mathbf{I} + \mathbf{G}^+ *)(\partial_x - 2\partial_s)\mathbf{R} + \mathbf{R} * \partial_x \mathbf{G}^+ - 2\mathbf{R}(x, +0)\mathbf{G}^+. \tag{5.7}$$

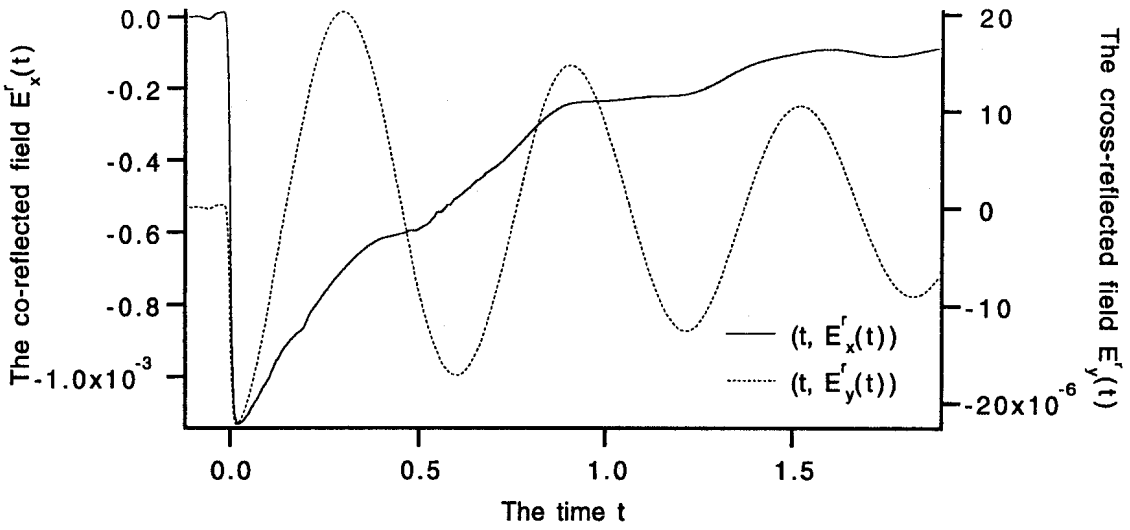


**Figure 16**: The graphs of components of the reflected electric field, $\boldsymbol{E}^r = (E^r_x, E^r_y)$, at the front wall of the Debye-Lorentz medium in Example 2 in Section 4. $\boldsymbol{E}^r$ has been obtained by the convolution of the reflection matrix kernel, $\mathbf{R}$, and the incident electric field at the front wall, $\boldsymbol{E}^i$, see Eq. (2.5). See also Figures 11 and 14. The time $t$ is given in units of $d/c$, and the scattered electric fields have the same unit as the incident electric field.

Furthermore, if the second relation in Eq. (5.3) is inserted in Eq. (5.2), then

$$-\partial_x \mathbf{G}^+ = (\mathbf{I} + \mathbf{G}^+ *)\partial_s \left\{\mathbf{G} + \mathbf{K} + (\mathbf{F} - \mathbf{L}) * \mathbf{R}\right\}. \tag{5.8}$$

Let the Volterra operator $\mathbf{I} + \mathbf{T}*$ act on this equation and use Eq. (5.6). The result is

$$(\mathbf{I} + \mathbf{G}^+ *)\partial_x \mathbf{T} = (\mathbf{I} + \mathbf{G}^+ *)\big((\mathbf{I} + \mathbf{T}*)\partial_s \left\{\mathbf{G} + \mathbf{K} + (\mathbf{F} - \mathbf{L}) * \mathbf{R}\right\}\big),$$

and since the inverse of $(\mathbf{I} + \mathbf{G}^+ *)$ exists,

$$\partial_x \mathbf{T} = (\mathbf{I} + \mathbf{T}*)\partial_s \left\{\mathbf{G} + \mathbf{K} + (\mathbf{F} - \mathbf{L}) * \mathbf{R}\right\}, \tag{5.9}$$

i.e., the transmission imbedding equation (5.5) holds for the functions $\mathbf{R}$ and $\mathbf{T}$ defined by Eq. (5.3). It remains to prove that these kernels also satisfy the reflection imbedding equation (5.4). To see this, let the Volterra operator $(\mathbf{I} + \mathbf{G}^+ *)^{-1}$ act on Eq. (5.1). By Eq. (5.7) and the second relation in Eq. (5.3) one obtains

$$\begin{aligned}(\partial_x - 2\partial_s)\mathbf{R} = &-(\mathbf{I} + \mathbf{G}^+ *)^{-1}\partial_x \mathbf{G}^+ * \mathbf{R} + \\ &+ (2\mathbf{R}(x,0) + \mathbf{F}(0) + \mathbf{L}(0))(\mathbf{I} + \mathbf{G}^+ *)^{-1}\mathbf{G}^+ + \\ &+ (\mathbf{G}(0) + \mathbf{K}(0))\mathbf{R} + \partial_s \left\{\mathbf{F} + \mathbf{L} + (\mathbf{G} - \mathbf{K}) * \mathbf{R}\right\}.\end{aligned} \tag{5.10}$$

Use of the initial condition $\mathbf{R}(x, +0) = \mathbf{G}^-(x, +0) = -(\mathbf{F}(+0) + \mathbf{L}(+0))/2$ and the substitution of Eq. (5.8) into Eq. (5.10) now yields the reflection imbedding equation (5.4), since the contributions involving the chirality kernel $\mathbf{K}$ cancel.

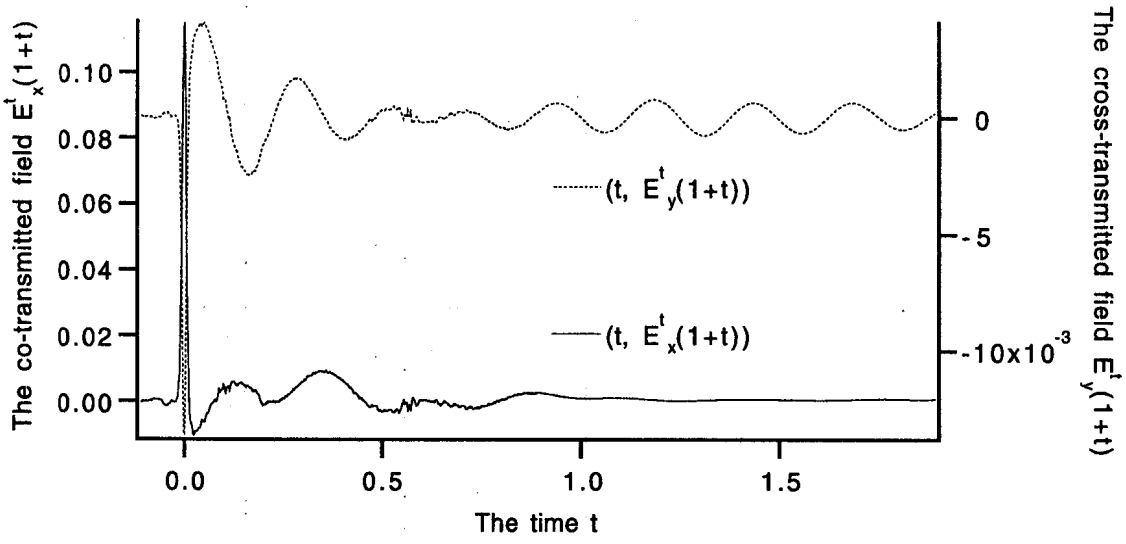


**Figure 17**: The graphs of components of the transmitted electric field, $\boldsymbol{E}^t = (E_x^t, E_y^t)$, at the back wall of the Debye-Lorentz medium in Example 2 in Section 4. $\boldsymbol{E}^t$ is obtained by the convolution of the transmission matrix kernel, $\mathbf{T}$, and the incident electric field at the front wall, $\boldsymbol{E}^i$, see Eq. (2.5). See also Figures 11 and 15. The time $t$ is given in units of $d/c$. Note the time translation (of half a roundtrip).

Conversely, assume that $\mathbf{R}$ and $\mathbf{T}$ satisfy the imbedding equations (5.4) and (5.5), and define $\mathbf{G}^{\pm}$ by Eq. (5.3). Then $\mathbf{G}^{\pm}$ satisfy the Green functions equations. To see this, let Eq. (5.5), or rather its equivalent, Eq. (5.9), be subject to the operator $(\mathbf{I} + \mathbf{G}^+ *)$. Application of Eq. (5.6) immediately yields the equation

$$-(\mathbf{I} + \mathbf{T}*)\partial_x \mathbf{G}^+ = (\mathbf{I} + \mathbf{T}^+ *)\big((\mathbf{I} + \mathbf{G}^+ *)\partial_s \{\mathbf{G} + \mathbf{K} + (\mathbf{F} - \mathbf{L}) * \mathbf{R}\}\big).$$

Since the inverse of the operator $(\mathbf{I} + \mathbf{T}*)$ exists, it follows that $\mathbf{G}^+$ satisfy Eq. (5.8), which easily can be transformed to the Green functions equation (5.2) by the second relation in Eq. (5.3). It is now possible to write the reflection imbedding equation (5.4) as in Eq. (5.10), and, finally, by letting the operator $\mathbf{I} + \mathbf{G}^+ *$ act on this equation, the Green functions equation (5.1) is also obtained. This completes the proof of the fact that the two formulations of the propagation problem can be transformed into one another by Eq. (5.3). Note also that initial values, boundary values, and jump discontinuities are transformed properly by Eq. (5.3), and that the derivation holds for the stratified slab.

The unique solution to the reflection imbedding equation is now derived. For the semi-infinite homogeneous bi-isotropic slab one readily obtains the non-linear Volterra equation

$$-2\mathbf{R}_\infty = \mathbf{F} + \mathbf{L} + 2\mathbf{G} * \mathbf{R}_\infty + (\mathbf{F} - \mathbf{L}) * \mathbf{R}_\infty * \mathbf{R}_\infty, \tag{5.11}$$

since the reflection kernel $\mathbf{R}_\infty$ is independent of $x$ in this case. This equation also holds for the finite slab in the triangular region bounded by the lines $s = 0$, $x = 0$, and $s = 2(1-x)$, where the presence of the back wall has not yet been observed. By

unique solvability, the property $(\mathbf{F}-\mathbf{L})*\mathbf{R}_\infty$ is proportional to the identity matrix. The proportionality factor is denoted by $R_{1,\infty}$, i.e., $R_{1,\infty}\mathbf{I}=(\mathbf{F}-\mathbf{L})*\mathbf{R}_\infty$, and this function satisfies

$$-2R_{1,\infty}=F*F+L*L+2G*R_{1,\infty}+R_{1,\infty}*R_{1,\infty}. \tag{5.12}$$

In each bounded interval $s\in(0,a)$, the solutions to Eqs. (5.12) and (5.11) can be obtained by successive approximations, and they are given by

$$R_{1,\infty}=-1-G+\sum_{n=0}^{\infty}\binom{\frac{1}{2}}{n}(2G+G^2-F^2-L^2)^n \tag{5.13}$$

and

$$\mathbf{R}_\infty=-(1+(G+\frac{R_{1,\infty}}{2})*)^{-1}\frac{(\mathbf{F}+\mathbf{L})}{2},$$

respectively, where the notation $G^n:=G*G*\cdots*G$ ($n-1$ times) with $G^0:=1$ and $G^1:=G$ has been adopted. Note that the lowest non-vanishing power of the susceptibility kernels in the series (5.13) is quadratic ($=-(F^2+L^2)/2$). This series converges absolutely and uniformly on $(0,a)$ by Weierstrass' comparison test since the terms are convolutions. Thus, term by term integration is justified. The inverse of the Volterra operator $1+(G+R_{1,\infty}/2)*$ can be written $1+f*$, where $f$ is the resolvent kernel to $G+R_{1,\infty}/2$, i.e.,

$$f+G+\frac{R_{1,\infty}}{2}+f*(G+\frac{R_{1,\infty}}{2})=0.$$

Naturally, the reflection kernel $\mathbf{R}_\infty$ can also be expressed as an absolutely and uniformly series on $(0,a)$ involving the susceptibility kernels $G$, $F$, and $L$:

$$\mathbf{R}_\infty=-\Big(1+\Big(\sum_{n=1}^{\infty}(G+\frac{R_{1,\infty}}{2})^n(-1)^n\Big)*\Big)\frac{(\mathbf{F}+\mathbf{L})}{2}. \tag{5.14}$$

Knowledge of $\mathbf{R}_\infty$ makes it possible to derive the general solution to the reflection imbedding equation also for $2(1-x)<s<a+2(1-x)$. To see this, define the deviation from $\mathbf{R}_\infty$ by $\Delta\mathbf{R}(x,s):=\mathbf{R}(x,s+2(1-x))-\mathbf{R}_\infty(s+2(1-x))$. This deviation is identically zero for $s<0$, and for $0<s<a$, it satisfies the boundary value problem

$$\begin{cases}\partial_x\Delta\mathbf{R}=\partial_s\left\{C*\Delta\mathbf{R}+(\mathbf{F}-\mathbf{L})*\Delta\mathbf{R}*\Delta\mathbf{R}\right\},\\ \Delta\mathbf{R}(1,s)=-\mathbf{R}_\infty(s),\end{cases} \tag{5.15}$$

where $C(s):=2(G(s)+R_{1,\infty}(s))$ only depends on time $s$. Define

$$\Delta R_1\mathbf{I}:=\partial_s\left\{(\mathbf{F}-\mathbf{L})*\Delta\mathbf{R}\right\}=(\mathbf{F}(0)-\mathbf{L}(0)+(\mathbf{F}'-\mathbf{L}')*)\Delta\mathbf{R}, \tag{5.16}$$

to obtain a scalar problem:

$$\begin{cases}\partial_x\Delta R_1=(C(0)+C'*)\Delta R_1+\Delta R_1*\Delta R_1,\\ \Delta R_1(1,s)=-R'_{1,\infty}(s).\end{cases} \tag{5.17}$$

This is, however, an equation of Riccati type, which can be linearized with the substitution $\partial_x U(x,s) = \big((1-U(x,\cdot)*)\Delta R_1(x,\cdot)\big)(s)$, where $U(1,\cdot) := 0$ without restriction. For each, with respect to $x$, continuously differentiable solution $\Delta R_1$ defined on $(x,s) \in (0,1)\times(0,a)$, this substitution determines uniquely a twice, with respect to $x$, continuously differentiable function $U$ on $(x,s) \in (0,1)\times(0,a)$, and vice versa. This follows from the expression

$$U(x,s) = -\sum_{n=1}^{\infty} \big( \int_1^x \Delta R_1(x',s)\,dx' \big)^n \frac{(-1)^n}{n!}$$

obtained by successive approximations and by

$$\Delta R_1(x,s) = \big((1-U(x,\cdot)*)^{-1}\partial_x U(x,\cdot)\big)(s). \tag{5.18}$$

Let $1-U*$ act on both sides of Eq. (5.17) and use the definition of $U$. Since $\partial_x U(1,s) = -R'_{1,\infty}(s)$ for all $s$, integration with respect to $x$ then yields

$$\begin{cases} \partial_x U + R'_{1,\infty} = (C(0) + C'*)U, \\ U(1,s) = 0. \end{cases}$$

The solution to this equation is

$$U(x,s) = -\Big(x - 1 + \Big(\sum_{n=2}^{\infty} (C(0)+C')^{n-1} \frac{(x-1)^n}{n!}\Big) * \Big) R'_{1,\infty},$$

where

$$(C(0)+C')^n := \sum_{k=0}^{n} \binom{n}{k} C(0)^{n-k} (C')^k.$$

(Recall the notation $(C')^k := C' * C' * \cdots * C'$ ($k-1$ times).) The solution (5.18) to the scalar problem (5.17) is therefore

$$\Delta R_1 = -\Big(1 + \Big(x - 1 + \Big(\sum_{n=2}^{\infty} (C(0)+C')^{n-1} \frac{(x-1)^n}{n!}\Big) * \Big) R'_{1,\infty} * \Big)^{-1} \Big(1 + \Big(\sum_{n=1}^{\infty} (C(0)+C')^{n} \frac{(x-1)^n}{n!}\Big) * \Big) R'_{1,\infty},$$

and using Eq. (5.16), it is now easy to verify that the solution to Eq. (5.15) is

$$\Delta \mathbf{R}(x,s) = -\mathbf{R}_\infty(s) - \Big\{ \sum_{n=1}^{\infty} \big( \int_1^x (C(0) + C'(\cdot) + \Delta R_1(x',\cdot))\,dx' \big)^n \frac{1}{n!} * \mathbf{R}_\infty(\cdot) \Big\}(s),$$

which establishes the solution

$$\mathbf{R}(x, s+2(1-x)) = \mathbf{R}_\infty(s+2(1-x)) + \Delta\mathbf{R}(x,s), \qquad 0 < s < a,$$

to the reflection imbedding equation in the rest of its domain of definition. Note that the solution is well-defined since the series involved converges absolutely and uniformly on $(x,s) \in (0,1) \times (0,a)$. Observe that these formulas show that the new information about the susceptibility kernels that one can extract from the (physical) reflection kernel $\mathbf{R}(s)$ is contained in the part $\mathbf{R}_\infty(s)$ only, just as expected.

Once the reflection imbedding kernel is known, it is easy to obtain the solution to the transmission imbedding equation (5.9):

$$\mathbf{T}(x,s) = \sum_{n=1}^{\infty} \Big( \int_1^x \partial_s \big( \mathbf{G}(s) + \mathbf{K}(s) + \{(\mathbf{F}-\mathbf{L}) * \mathbf{R}\}(x',s) \big)\, dx' \Big)^n \frac{1}{n!}.$$

Similarly, the Green functions can be solved:

$$\begin{cases} \mathbf{G}^+(x,s) = \displaystyle\sum_{n=1}^{\infty} \Big( \int_0^x \partial_s \big( \mathbf{G}(s) + \mathbf{K}(s) + \{(\mathbf{F}-\mathbf{L}) * \mathbf{R}\}(x',s) \big)\, dx' \Big)^n \frac{(-1)^n}{n!}, \\ \mathbf{G}^-(x,s) = \mathbf{R}(x,s) + \big( \mathbf{R}(x,\cdot) * \mathbf{G}^+(x,\cdot) \big)\,(s). \end{cases}$$

The first formula is obtained from Eq. (5.8) and the second is just the second formula in Eq. (5.3). The formula for $\mathbf{G}^-$ and the remark at the end of the preceding paragraph show that the second formula in Eq. (3.3) follows from the first term in the series (5.14). The first term in the series for $\mathbf{G}^+(1,s) = \mathbf{T}(s)$ shows that the first formula in Eq. (3.3) holds. This completes the investigation.

# 6 Conclusion

In this paper, a non-iterative method to reconstruct a finite time trace of the four susceptibility kernels of a general dispersive, homogeneous bi-isotropic slab is presented. Finite time traces of the reflected and transmitted fields induced by a normally incident electromagnetic pulse are used as data. Deconvolution reduces the problem to the generic one, which has been investigated before. An improved version of the inverse algorithm is used in this paper. In a couple of numerical examples, it is demonstrated that it is possible to obtain very good reconstructions of the dispersive properties of the bi-isotropic medium, in spite of the ill-posed nature of deconvolution. Finally, the exact solution to the direct scattering problem is derived for arbitrary susceptibility kernels, and its explicit form (series expansions) supports the employed inverse algorithm.

# 7 Acknowledgment

The work reported in this paper is supported by a grant from the Swedish Research Council for Engineering Sciences, and its support is gratefully acknowledged.

# References


[1] J.P. Corones, G. Kristensson, P. Nelson, and D.L. Seth, editors. *Invariant Imbedding and Inverse Problems*. SIAM, 1992.

[2] N. Engheta and D.L. Jaggard. Electromagnetic chirality and its applications. *IEEE Antennas and Propagation Society Newsletter*, pages 6–12, October 1988.

[3] J Fridén. Inverse scattering for anisotropic mirror image symmetric media. *Inverse Problems*. (in press).

[4] J. Fridén, G. Kristensson, and R.D. Stewart. Transient electromagnetic wave propagation in anisotropic dispersive media. *J. Opt. Soc. Am. A*, **10**(12), 2618–2627, 1993.

[5] P. Fuks, A. Karlsson, and G. Larson. Direct and inverse scattering for dispersive media. *Inverse Problems*, **10**(3), 555–571, 1994.

[6] P. Fuks, G. Kristensson, and G. Larson. Permittivity profile reconstructions using transient electromagnetic reflection data. Technical Report LUTEDX/(TEAT-7009)/1–88/(1989), Lund Institute of Technology, Department of Electromagnetic Theory, P.O. Box 118, S-211 00 Lund, Sweden, 1990.

[7] A. Karlsson. Inverse scattering for viscoelastic media using transmission data. *Inverse Problems*, **3**, 691–709, 1987.

[8] A. Karlsson and G. Kristensson. Constitutive relations, dissipation and reciprocity for the Maxwell equations in the time domain. *J. Electro. Waves Applic.*, **6**(5/6), 537–551, 1992.

[9] G. Kristensson and S. Rikte. The inverse scattering problem for a homogeneous bi-isotropic slab using transient data. In L. Päivärinta and E. Somersalo, editors, *Inverse Problems in Mathematical Physics*, pages 112–125. Springer, Berlin, 1993.

[10] G. Kristensson and S. Rikte. Transient wave propagation in reciprocal bi-isotropic media at oblique incidence. *J. Math. Phys.*, **34**(4), 1339–1359, 1993.

[11] A. Lakhtakia. Recent contributions to classical electromagnetic theory of chiral media: what next? *Speculations in Science and Technology*, **14**(1), 2–17, 1991.

[12] S. Rikte. Causality theorems and Green functions for transient wave propagation problems in stratified complex media. Technical Report LUTEDX/(TEAT-7029)/1–17/(1994), Lund Institute of Technology, Department of Electromagnetic Theory, P.O. Box 118, S-211 00 Lund, Sweden, 1994.

[13] M.M.I. Saadoun and N. Engheta. A reciprocal phase shifter using noval pseudochiral or $\Omega$ medium. *Microwave and Optical Technology Letters*, **5**(4), 184–187, 1992.